

## Selectively excited emission and $Tb^{3+} \rightarrow Ce^{3+}$ energy transfer in yttrium aluminum garnet

Xingren Liu, Xiaojun Wang, and Zhongkai Wang

Changchun Institute of Physics, Academia Sinica, Changchun 130021, China

(Received 5 October 1988)

Selectively excited emission and  $Tb^{3+} \rightarrow Ce^{3+}$  energy transfer in  $Y_3Al_5O_{12}:Tb,Ce$  (YAG:Tb,Ce) at room temperature were studied. The selective excitation included a 266.0-nm laser pulse. The processes of  $Tb^{3+} \rightarrow Ce^{3+}$  radiative and nonradiative energy transfer occur simultaneously in YAG:Tb,Ce. The mechanism of nonradiative energy transfer from the  $Tb^{3+} {}^5D_3$  and  ${}^5D_4$  levels to the  $Ce^{3+} {}^2D_{3/2}$  state was found to be the dipole-dipole interaction. The average critical transfer distances  $R_0$  were 15.1 Å for  ${}^5D_3(Tb^{3+})$  and 15.4 Å for  ${}^5D_4(Tb^{3+})$ , respectively. The rates and efficiencies were obtained.

### I. INTRODUCTION

With the advance in knowledge of lasers and luminescence, most of the interest in  $Y_3Al_5O_{12}$  (YAG) has concerned its use as a host material for a number of rare-earth lasers and phosphors.<sup>1</sup>  $Ce^{3+}$ -activated YAG, for example, gives a fast flying-spot-scanner phosphor.<sup>2</sup> Since the host material has high thermal conductivity the  $Tb^{3+}$ -activated  $Y_3Al_5O_{12}$  garnet is suitable for operation under high-energy electron bombardment and cathode-ray-tube (CRT) displays under high ambient illumination.<sup>3,4</sup> YAG:Ce crystal has also been considered as a laser medium under flashlamp pumping.<sup>5</sup>

Energy transfer from donor to acceptor plays an important role in luminescence and in solid-state lasers. Energy-transfer mechanisms between  $Ce^{3+}$  and  $Nd^{3+}$  in YAG:Nd,Ce at low temperature have been studied.<sup>6</sup> Energy-transfer phenomena and mechanisms for  $Ce^{3+}$ -to- $Tb^{3+}$  transfer have been extensively investigated in many compounds involving borates, aluminates, phosphates, silicates, and fluorides.<sup>7-12</sup>

In studying the fluorescence properties of the  $Ce^{3+}$  and  $Tb^{3+}$  codoped  $Y_3Al_5O_{12}$  and  $Y_3Ga_5O_{12}$  garnets, energy transfer from  $Tb^{3+}$  to  $Ce^{3+}$  was observed by Liu and co-workers for short-wavelength excitation containing a 266.0-nm laser pulse with a width of 10 ns at room temperature.<sup>13-15</sup> A new excitation band corresponding to the  $4f \rightarrow 5d$  transition of  $Tb^{3+}$  occurred in the excitation spectrum of  $Ce^{3+}$  emission in YAG:Ce,Tb.<sup>13</sup> Recently,  $Tb^{3+} \rightarrow Ce^{3+}$  energy transfer in YAG:Ce,Tb single-crystal films made by liquid-phase epitaxy was studied using pulsed electron-beam excitation.<sup>16</sup>

In this paper, selectively excited emissions and  $Tb^{3+} \rightarrow Ce^{3+}$  radiative and nonradiative energy transfer have been investigated at room temperature under different excitation, including 266.0-nm laser pulses of 10-ns duration. The mechanism for nonradiative energy transfer from the  ${}^5D_3$  and  ${}^5D_4$  levels of  $Tb^{3+}$  to the lowest  $5d$  state  ${}^2D_{3/2}$  of  $Ce^{3+}$  was found to be electric dipole-dipole interaction. The experimental results were fitted to the Inokuti-Hirayama equation. Electric dipole-quadrupole interactions could be neglected.

### II. THEORETICAL BACKGROUND

For radiative transfer, photons emitted by the donor are reabsorbed by any coactivator (acceptor). The pattern of donor fluorescence depends on the acceptor concentration, but the donor lifetime does not change with acceptor concentration.<sup>17</sup> The probability  $P_{DA}$  for such transfer is given by the formula

$$P_{DA} = \frac{\sigma_A}{4R^2} \frac{1}{\tau_0} \int f_D(E) f_A(E) dE, \quad (1)$$

where  $\sigma_A$  is integrated absorption cross section of the acceptor ( $A$ ),  $R$  is the distance between  $D$  and  $A$  ions,  $\tau_0$  is the acceptor lifetime, and  $f_D(E)$  and  $f_A(E)$  are the normalized fluorescence spectrum of the donor ( $D$ ) and the normalized absorption spectrum of the acceptor, respectively.

Nonradiative energy transfer between donor and acceptor ions arises from multipolar or exchange interactions.

The theory of nonradiative energy transfer from one donor to another acceptor has been discussed in detail by several authors. The preliminary explanation was given by Forster, and Dexter applied the theory to energy transfer between ions in inorganic solids.<sup>18,19</sup> The nature of the donor fluorescence decay was analyzed by Inokuti and Hirayama.<sup>20</sup> Yokota and Tanimoto<sup>21</sup> treated the problem taking into account the diffusion of energy among donor ions.

For no energy diffusion among donor ions, the intensity of donor fluorescence  $I(t)$  for electric multipolar interactions is given by the Inokuti-Hirayama formula<sup>20</sup>

$$I(t) = I(0) \exp \left[ -\frac{t}{\tau_0} - \frac{4}{3} \pi \Gamma \left[ 1 - \frac{3}{s} \right] N_A R_0^3 \left[ \frac{t}{\tau_0} \right]^{3/s} \right], \quad (2)$$

where  $\tau_0$  is the intrinsic lifetime of the donor ion,  $N_A$  the concentration of acceptor ions,  $\Gamma$  the gamma function,  $R_0$  the critical transfer distance, and  $s$  the interaction parameter equal to 6 for dipole-dipole, 8 for dipole-quadrupole and 10 for quadrupole-quadrupole interaction.

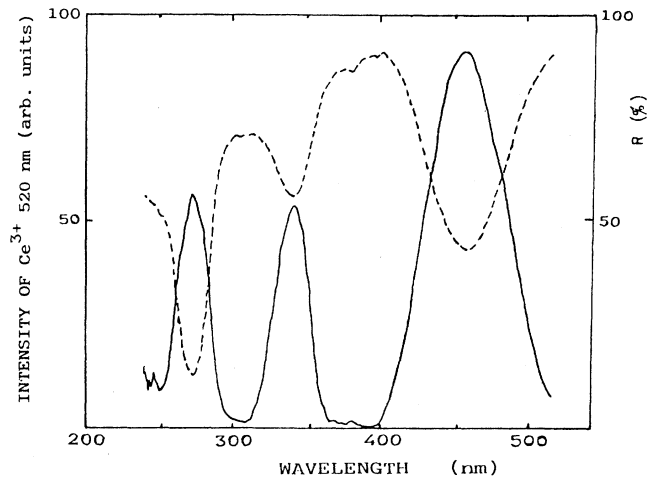


FIG. 1. Diffuse reflection spectrum (dotted curve) of  $Y_3Al_5O_{12}:Tb,Ce$  and excitation spectrum (solid curve) of the  $Ce^{3+}$  520-nm emission in  $Y_3Al_5O_{12}:Tb,Ce$ .

### III. EXPERIMENT

Samples of the composition  $(Y_{0.99-x}Tb_{0.01}Ce_x)_3Al_5O_{12}$  were prepared by solid-state reaction at high temperature. The starting materials were high-purity powders. Stoichiometric amounts of  $Y_2O_3$ ,  $Al_2O_3$ ,  $Tb_4O_7$ , and  $CeO_2$  or other cerium compounds were mixed with a fluoride flux. The mixture was fired at  $1450^\circ C$  for 3 h in a closed alumina crucible. The resulting product was a green-yellow powder.

Excitation and fluorescence spectra were measured at room temperature on a Perkin-Elmer Spectrofluorometer MPF-4A with a 75-W xenon lamp. The diffuse reflection spectrum of the samples was measured relative to  $MgO$ .

266.0-nm laser pulses with a width of 10 ns, obtained

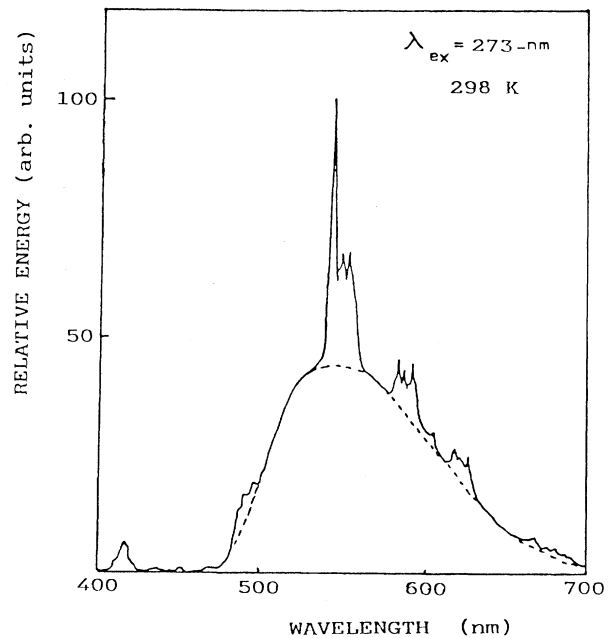


FIG. 3. Spectral energy distribution of the emission of the  $Y_3Al_5O_{12}:Ce,Tb$  garnet for excitation at 273 nm.

by fourth-harmonic generation of a YAG:Nd laser, were used for pulse excitation. The emission was focused onto the entrance slit of a type GDM-1000 monochromator with a cooled photomultiplier tube type M12FC51. Emissions at 418.0 and 544.0 nm corresponding to the  $Tb^{3+} {}^5D_3 \rightarrow {}^7F_5$  and  ${}^5D_4 \rightarrow {}^7F_5$  transitions were analyzed by means of a BX-530A boxcar integrator. The boxcar window was scanned to determine the fluorescence lifetimes of the  $Tb^{3+}$  ions in  $Y_3Al_5O_{12}:Ce,Tb$  garnets. All measurements were made at room temperature.

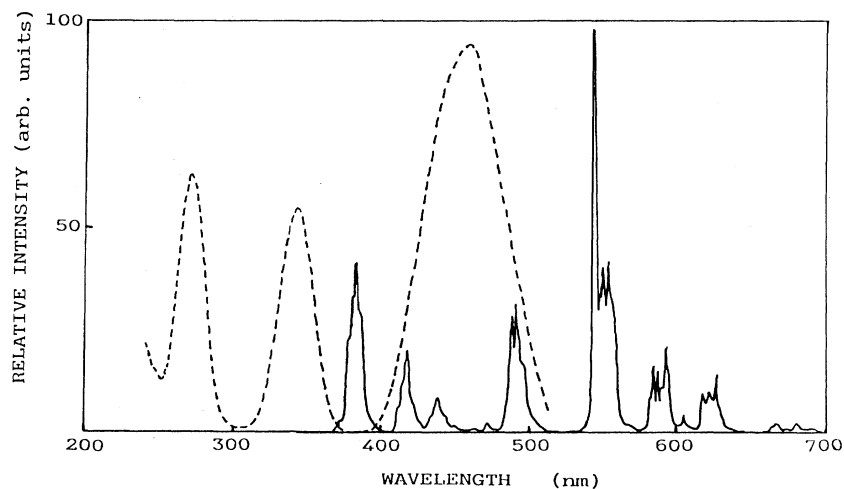


FIG. 2. Excitation spectrum of the  $Ce^{3+}$  520-nm emission in YAG:Tb,Ce (dashed curve) and emission spectrum of  $Tb^{3+}$  in YAG:Tb (solid curve) under 275-nm excitation.

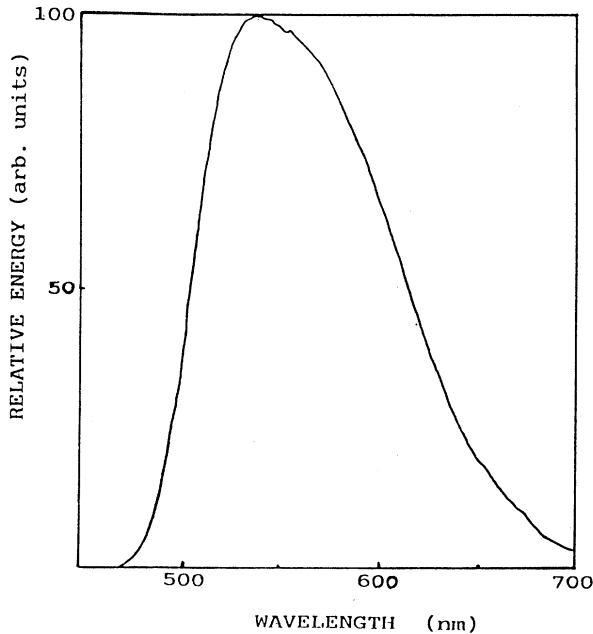


FIG. 4. Spectral energy distribution of the emission of  $Y_3Al_5O_{12}:Ce,Tb$  under 450-nm excitation.

#### IV. RESULTS

The diffuse reflection spectrum of YAG codoped with  $Ce^{3+}$  and  $Tb^{3+}$  is shown in Fig. 1 (dotted curve). This reflection spectrum consists of three strong broad bands and very weak lines. The broad band at approximately 275 nm in the short-wavelength region and the narrow lines in the 360–400-nm spectral region correspond, respectively, to the  $4f-5d$  and  $4f-4f$  transitions of  $Tb^{3+}$ ; the two broad bands from 310 to 380 nm in the long-wavelength uv region and from 400 to 520 nm in the blue spectral region correspond to the  $4f-5d$  transitions of

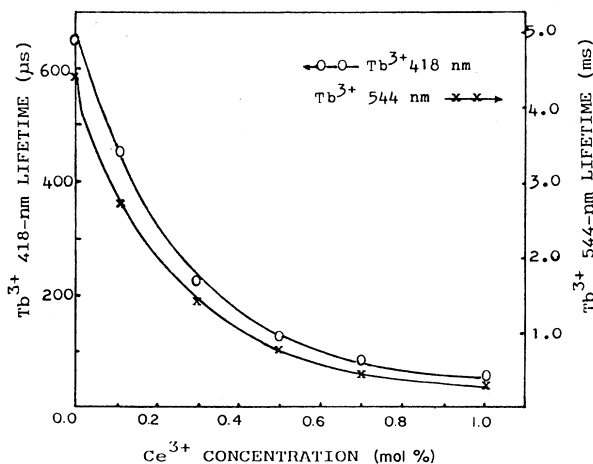


FIG. 5. Fluorescence lifetimes at 298 K for the  ${}^5D_3 \rightarrow {}^7F_5$  (418-nm) and  ${}^5D_4 \rightarrow {}^7F_5$  (544-nm) transitions of  $Tb^{3+}$  in  $YAG-0.01 \text{ mol } \% Tb,xCe$  as a function of  $Ce^{3+}$  concentration.

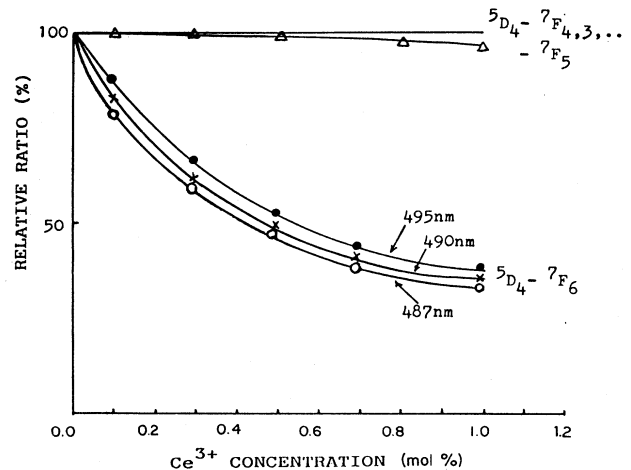


FIG. 6. Ce concentration dependence of the relative ratio of the fluorescence branches of  $I({}^5D_4-{}^7F_6)/I({}^5D_4-{}^7F_4)$  and  $I({}^5D_4-{}^7F_{5,4,\dots})/I({}^5D_4-{}^7F_4)$  in  $YAG-0.01 \text{ mol } \% Tb,xCe$ .

$Ce^{3+}$  in YAG.<sup>2,5,13</sup> The solid curve in Fig. 1 shows the excitation spectrum of the  $Ce^{3+}$  520-nm emission in  $YAG:Ce,Tb$ . This excitation spectrum agrees with the absorption spectrum of  $Ce^{3+}$  and  $Tb^{3+}$  in  $YAG:Ce,Tb$ . In particular, the strong excitation (or absorption) band corresponding to the  $Tb^{3+} 4f-5d$  absorption occurs in the excitation spectrum of the  $Ce^{3+}$ . Since this excitation is absorbed in  $Tb^{3+}$  but is emitted by  $Ce^{3+}$ ,  $Tb^{3+} \rightarrow Ce^{3+}$  energy transfer is implied.

In YAG, the  $Tb^{3+}$  (donor) emission spectrum and the  $Ce^{3+}$  (acceptor) excitation spectrum overlap considerably; see Fig. 2. Radiative and nonradiative transfer can occur by reabsorption and electric multipolar interaction.  $Y_3Al_5O_{12}$  activated only by  $Ce^{3+}$  does not fluoresce when excited in the 250–290-nm region. However, in the presence of  $Tb^{3+}$ , strong  $Ce^{3+}$  emission is induced. For selective excitation by short-wavelength uv radiation, the fluorescence spectrum of  $YAG:Ce,Tb$  consists of a broad band, corresponding to the  $Ce^{3+} 5d \rightarrow {}^2F_j$  transition, and

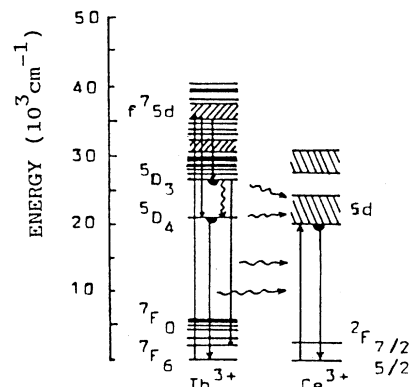


FIG. 7. Energy-level diagrams and transfer pathways for  $Tb^{3+}$  and  $Ce^{3+}$  in  $Y_3Al_5O_{12}$  garnet.

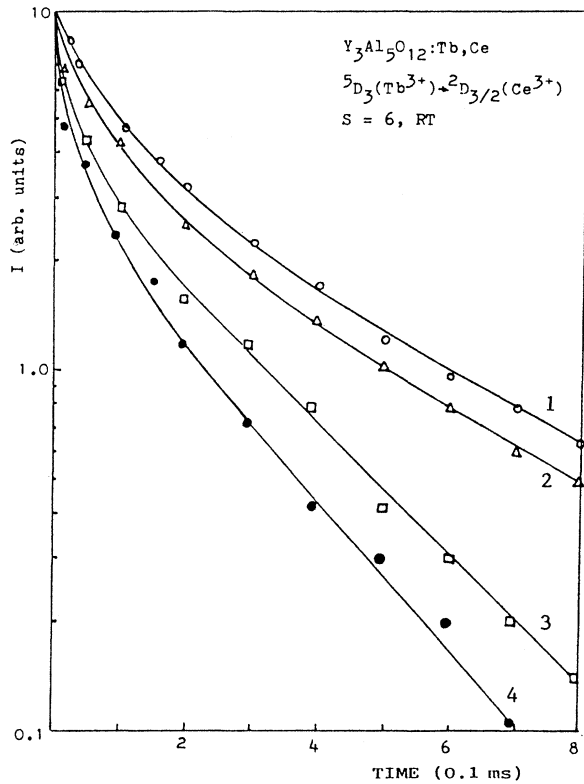


FIG. 8. Fluorescence decay patterns of the  ${}^5D_3$  (418-nm) emission of  $Tb^{3+}$  as a function of  $Ce^{3+}$  concentration in YAG-0.01 mol %  $Tb,xCe$  at 298 K.  $x=0.3$  mol % (no. 1), 0.5 mol % (no. 2), 0.7 mol % (no. 3), and 1.0 mol % (no. 4). Solid curves, IH theoretical curves; the four symbols indicate the actual experimental values.

of two series of sharp lines corresponding to  $Tb^{3+}$   ${}^5D_3 \rightarrow {}^7F_J$  and  ${}^5D_4 \rightarrow {}^7F_J$  ( $J=6,5,\dots,0$ ) transitions. Figure 3 gives this energy distribution of the emission spectra of YAG:Ce,Tb for 273-nm uv excitation at 298 K. For long-wavelength uv and blue-region excitation, the  $Ce^{3+}$  ions are directly excited into their  $5d$  states, and the energy absorbed by the  $Tb^{3+}$  ions in these regions is unimportant. The fluorescence spectrum of  $Y_3Al_5O_{12}:Ce,Tb$  then consists mainly of a broad band extending from 470 to 700 nm corresponding to the  $Ce^{3+}$   $5d \rightarrow {}^7F_{5/2}, {}^7F_{7/2}$  transitions (see Fig. 4).

The fluorescence lifetime of the  $Tb^{3+}$  ions changes because of the interaction between  $Tb^{3+}$  and  $Ce^{3+}$  ions in

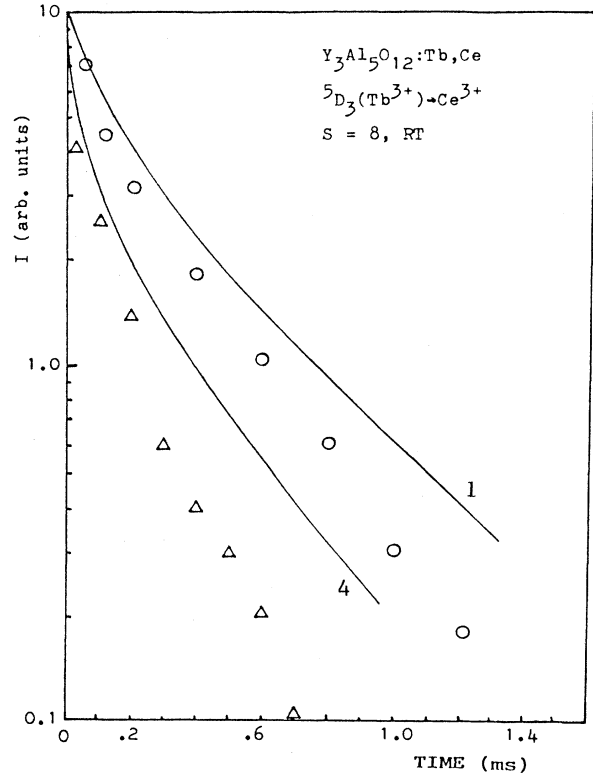


FIG. 9. Fluorescence decay of the  ${}^5D_3$  (418-nm) line of  $Tb^{3+}$  in YAG-0.01 mol %  $Tb,xCe$ . IH theoretical curves (solid lines) for  $S=8$ , and experimental values ( $\circ, \Delta$ ).

YAG:Ce,Tb. Figure 5 shows that the fluorescence lifetimes of the  $Tb^{3+}$   ${}^5D_3$  and  ${}^5D_4$  levels decreased with the  $Ce^{3+}$  concentration for excitation with the 266.0-nm laser pulse.

## V. DISCUSSION

### A. $Tb^{3+} \rightarrow Ce^{3+}$ radiative transfer

It is observed that the relative intensities of the  $Tb^{3+}$   ${}^5D_3$  and  ${}^5D_4 \rightarrow {}^7F_J$  emissions are different for YAG:Tb (see Fig. 2) and YAG:Ce,Tb (see Fig. 3). Figures 1 and 2 show that there is excellent overlap of the  $Tb^{3+}$   ${}^5D_3 \rightarrow {}^7F_J$  ( $J=6,5,\dots,0$ ) emission series and of the  ${}^5D_4 \rightarrow {}^7F_6$  emission line with the lowest absorption band of  $Ce^{3+}$ , i.e., the  $4f^2F_J$  ( $J=\frac{5}{2}, \frac{7}{2}$ )  $\rightarrow 5d$  transitions. This

TABLE I.  ${}^5D_3$  lifetimes and energy-transfer parameters of  $Tb^{3+}$  in YAG:Tb,Ce at 300 K.

| No.  | Tb conc.<br>(mol %) | Ce conc.<br>(mol %) | $\tau$ (418 nm)<br>( $\mu s$ ) | $\eta$ | $\omega$<br>( $10^3 s^{-1}$ ) | $R_0$<br>( $\text{\AA}$ ) |
|------|---------------------|---------------------|--------------------------------|--------|-------------------------------|---------------------------|
| 0    |                     | 0                   | 650                            |        |                               |                           |
| 1    | fixed at            | 0.3                 | 228                            | 0.65   | 2.85                          | 16.4                      |
| 2    | 1.0                 | 0.5                 | 128                            | 0.83   | 6.28                          | 14.7                      |
| 3    |                     | 0.7                 | 78                             | 0.88   | 11.28                         | 14.9                      |
| 4    |                     | 1.0                 | 44                             | 0.93   | 21.19                         | 14.4                      |
| avg. |                     |                     |                                |        |                               | 15.1                      |

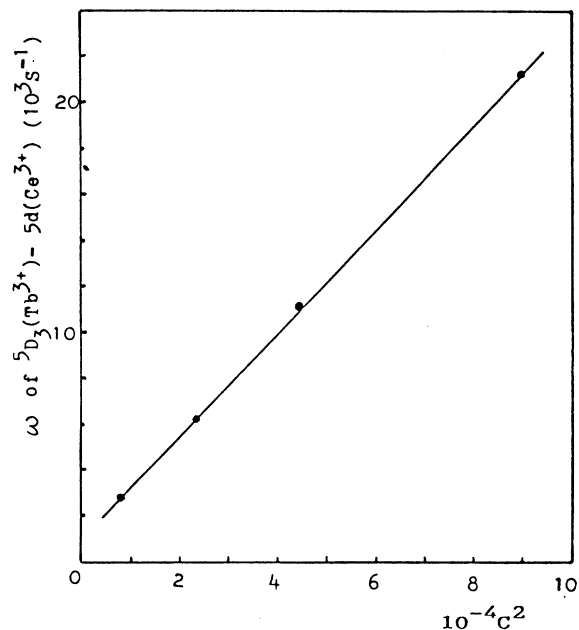


FIG. 10. Linear variation of the energy-transfer rate from the  $^5D_3$  level of  $Tb^{3+}$  to the  $5d$  state of  $Ce^{3+}$ , vs the square of the  $Ce^{3+}$  concentration, for YAG-0.01 mol %  $Tb_xCe$  phosphors.

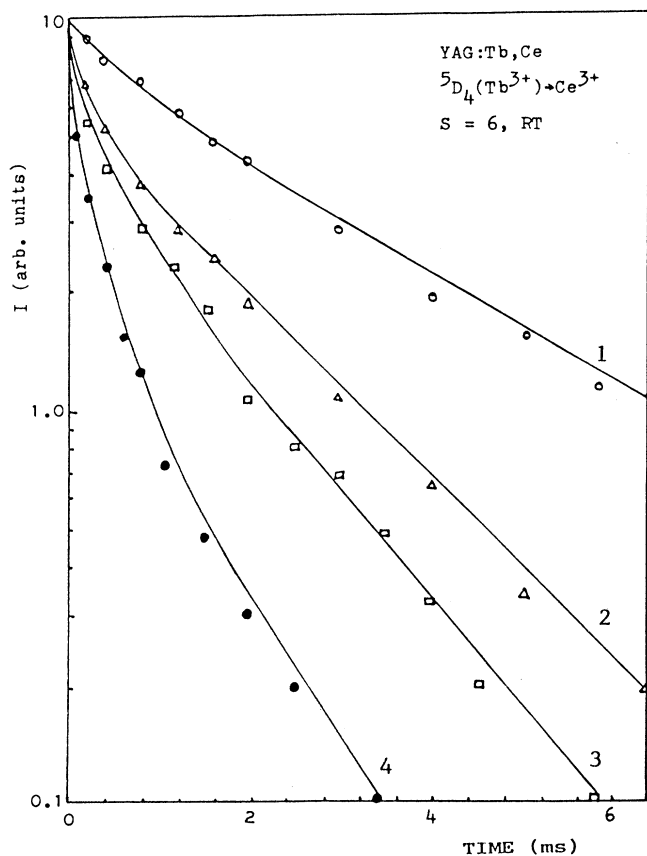


FIG. 11. Fluorescence decay patterns of the  $^5D_4$  (544-nm) emission of  $Tb^{3+}$ , as a function of  $Ce^{3+}$  concentration in YAG-0.01 mol %  $Tb_xCe$ .

overlap can cause radiative energy transfer by reabsorption. The evidence for the radiative transfer is provided by the relative branching ratios of the fluorescence transitions,  $I(^5D_4 \rightarrow ^7F_6)/I(^5D_4 \rightarrow ^7F_4)$  and  $I(^5D_4 \rightarrow ^7F_J)/I(^5D_4 \rightarrow ^7F_4)$  ( $J=5,4,\dots$ ), with increasing  $Ce^{3+}$  concentration. The  $^5D_4 \rightarrow ^7F_4$  (592-nm) transition was chosen as the reference branch because of its distance from the  $Ce^{3+}$  absorption band.

Under the excitation at 270 nm, the intensity ratio of  $I(^5D_4 \rightarrow ^7F_6)_{490 \text{ nm}}/I(^5D_4 \rightarrow ^7F_4)_{592 \text{ nm}}$  in YAG-1 mol % Tb is about 1.47 but is about 0.59 with 0.7 mol % Ce present. On the other hand, the relative branching ratios of the fluorescence transitions,  $I(^5D_4 \rightarrow ^7F_J)/I(^5D_4 \rightarrow ^7F_4)$  ( $J=5,4,3,\dots$ ), do not change with or without  $Ce^{3+}$  in YAG:Tb samples. Figure 6 shows the variations of the relative ratios of the fluorescence branches of  $Tb^{3+}$  ions. These ratios were normalized relative to those without  $Ce^{3+}$ . Three emission lines of 487, 490, and 495 nm represent the  $^5D_4 \rightarrow ^7F_6$  transition of  $Tb^{3+}$ . Figure 6 shows that the intensities of the three emission lines drop off gradually with increasing Ce concentration due to  $Tb^{3+} \rightarrow Ce^{3+}$  radiative energy transfer. The small differences among the three lines are due to the absorption spectrum of  $Ce^{3+}$ .

#### B. $^5D_3(Tb^{3+}) \rightarrow ^2D_{3/2}(Ce^{3+})$ nonradiative transfer

Before discussing the mechanisms of energy transfer between  $Tb^{3+}$  and  $Ce^{3+}$  in yttrium aluminum garnet, it is

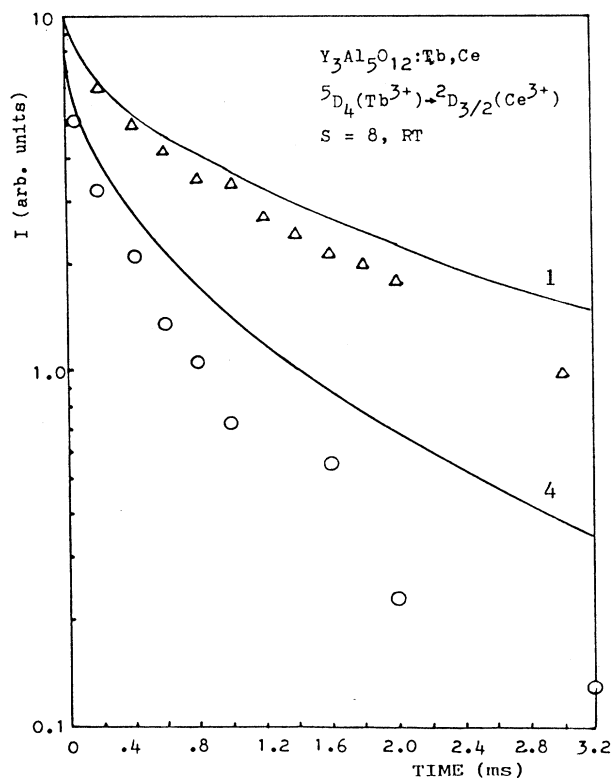


FIG. 12. Predicted fluorescence decay of the  $^5D_4$  (544-nm) emission of  $Tb^{3+}$  in YAG-0.01 mol %  $Tb_xCe$  for  $S=8$ , contrasted with the observed decay at room temperature.

important to consider the nature of the transitions of the  $\text{Tb}^{3+}$  and  $\text{Ce}^{3+}$  ions. Energy-level diagrams of these ions in YAG garnet are shown in Fig. 7. The  $\text{Ce}^{3+}$  emission is an allowed  $4f^05d^1-4f^15d^0$  transition of electric dipole character. We can see from Figs. 2 and 7 that the  $\text{Tb}^{3+}$   $^5D_3, ^5D_4 \rightarrow ^7F_J$  transitions and the  $\text{Ce}^{3+}$   $^2F \rightarrow$  lowest- $5d$ -excited-state transitions are in resonance. Short-wavelength uv excitation is efficiently absorbed by  $\text{Tb}^{3+}$  ions. The  $\text{Tb}^{3+}$  centers are first excited into the  $f^75d$  state and then relax very quickly nonradiatively to the  $^5D_3$  and  $^5D_4$  levels. It is reasonable to assume that energy transfer is primarily due to interaction between the  $^5D_3$  and  $^5D_4$  levels of  $\text{Tb}^{3+}$  and the lowest  $5d$  state of  $\text{Ce}^{3+}$ .

At the low donor ( $\text{Tb}^{3+}$ ) concentration used (1.0 mol %), the diffusion of excitation energy between  $\text{Tb}^{3+}$  ions can be neglected.<sup>21</sup> Therefore, the Inokuti-Hiroyama (IH) formula (2) can be used to describe the time evolution of the population density of the  $\text{Tb}^{3+}$  (donor) in the presence of the acceptor ( $\text{Ce}^{3+}$ ). The comparison between the experimental decay curve and the theoretical expression is used to determine the interaction parameter  $S$  of the multipolar interactions.

For  $\text{Tb}^{3+}(^5D_3) \rightarrow \text{Ce}^{3+} 5d(^2D_{3/2})$  transfer, the decay of  $\text{Tb}^{3+}$  418-nm emission ( $^5D_3 \rightarrow ^7F_5$ ) was used to monitor the decay of the  $\text{Tb}^{3+}$   $^5D_3$  level. The IH formula (2) was used to fit the experimental decays first for dipole-dipole coupling ( $S=6$ ) in Fig. 8 and then for dipole-quadrupole ( $S=8$ ) in Fig. 9. The fits were obtained by the standard least-squares method. Experimental decay results are shown for four samples of YAG-0.01 mol Tb, $x$ Ce, where  $x=0.3$  mol % (no. 1, 0), 0.5 mol % (no. 2,  $\Delta$ ), 0.7 mol % (no. 3,  $\square$ ), and 1.0 mol % (no. 4,  $\bullet$ ). The solid curves are the fitted theoretical IH curves. The best fit to the experimental points is obtained for  $S=6$  in Fig. 8. For higher  $\text{Ce}^{3+}$  concentration, more  $\text{Ce}^{3+}$  ions are close to donor  $\text{Tb}^{3+}$  ions, and the decay shows more nonexponentiality at early times and the lifetime is shorter. The experimental points deviated from the theoretical curves for  $S=8$  (dipole-quadrupole interaction). These results indicate that the dipole-dipole interaction is the mechanism governing nonradiative energy transfer from  $^5D_3(\text{Tb}^{3+})$  to  $^2D_{3/2}(\text{Ce}^{3+})$  in YAG:Tb,Ce under short-wavelength uv radiation. The critical energy-transfer distance ( $R_0$ ) was regarded as an adjustable parameter and gave an average critical distance of  $R_0=15.1$  Å. The critical distance was obtained by Shmulovich *et al.*<sup>16</sup> as 18 Å for the case of pulsed cathode-ray excitation. The measured values of

the lifetimes and the derived values of the critical distance are listed in Table I. The rates ( $\omega$ ) and efficiencies ( $\eta$ ) of nonradiative energy transfer were calculated from the lifetime data using the expressions

$$\omega = \tau^{-1} - \tau_0^{-1} = \tau_0^{-1} (R_0/R_{sa})^6, \quad (3)$$

$$\eta = 1 - (\tau/\tau_0) = \omega/\tau^{-1}, \quad (4)$$

where  $\tau_0$  is the intrinsic lifetime of the donor and  $\tau$  is the lifetime of the donor in the presence of the acceptor.  $R_{sa}$  is the distance between donor and acceptor. The values obtained for  $\omega$  and  $\eta$  at room temperature (RT) are also presented in Table I. Additional evidence for the dipole-dipole mechanism of energy transfer is obtained by plotting the transfer rate ( $\omega$ ) versus the square of acceptor concentration<sup>22</sup> as shown in Fig. 10, which gives a straight line.

#### C. $^5D_4(\text{Tb}^{3+}) \rightarrow ^2D_{3/2}(\text{Ce}^{3+})$ nonradiative transfer

The fluorescence lifetimes of the  $^5D_4 \rightarrow ^7F_5$  (544-nm) transition of  $\text{Tb}^{3+}$  in  $(\text{Y}_{0.99-x}\text{Tb}_{0.01}\text{Ce}_x)_3\text{Al}_5\text{O}_{12}$  samples with different Ce concentrations are shown in Fig. 5. As discussed for the  $\text{Tb}^{3+}(^5D_3) \rightarrow \text{Ce}^{3+}$  transfer, the best fits of Eq. (2) to the experimental data assuming dipole-dipole interaction ( $S=6$ ) are shown by the solid lines in Fig. 11. The four type of symbols represent  $\text{Tb}^{3+}$  (544-nm) experimental decay values in YAG-0.01 mol Tb, $x$ Ce.

The fittings between experimental decay and the theoretical expression for dipole-quadrupole and quadrupole-quadrupole interactions are worse than for dipole-dipole interactions. Figure 12 shows the poor fit between  $^5D_4$  experimental and theoretical values for  $S=8$  (dipole-quadrupole interaction). Furthermore, a plot of  $\omega$  versus  $C^2$ , which gives a straight line, suggests nonradiative transfer via dipole-dipole interaction. Therefore, the resonance mechanism for  $^5D_4(\text{Tb}^{3+}) \rightarrow ^2D_{3/2}(\text{Ce}^{3+})$  transfer is dominated by the dipole-dipole interaction in the system YAG:Tb,Ce for short-wavelength uv pulse excitation. The dipole-quadrupole interaction can be neglected. Shmulovich *et al.*<sup>16</sup> in their work with pulsed electron-beam excitation of YAG:Tb,Ce crystal regarded transfer from the  $^5D_4(\text{Tb}^{3+})$  level to be governed by dipole-dipole interaction, but could also be described by dipole-quadrupole coupling.

The average critical transfer distance obtained by the method here is  $R_0=15.4$  Å. The rates ( $\omega$ ) and efficiencies ( $\eta$ ) for  $^5D_4(\text{Tb}^{3+}) \rightarrow \text{Ce}^{3+}$  transfer are given in Table II.

TABLE II.  $^5D_4$  lifetimes and energy-transfer parameters of  $\text{Tb}^{3+}$  in YAG:Tb,Ce at 300 K.

| No.  | Tb conc.<br>(mol %) | Ce conc.<br>(mol %) | $\tau$ (544 nm)<br>(ms) | $\eta$ | $\omega$<br>( $10^2 \text{ s}^{-1}$ ) | $R_0$<br>(Å) |
|------|---------------------|---------------------|-------------------------|--------|---------------------------------------|--------------|
| 0    |                     | 0                   | 4.40                    |        |                                       |              |
| 1    | fixed at            | 0.3                 | 1.42                    | 0.68   | 4.77                                  | 14.1         |
| 2    | 1.0                 | 0.5                 | 0.79                    | 0.82   | 10.39                                 | 16.9         |
| 3    |                     | 0.7                 | 0.49                    | 0.90   | 18.14                                 | 14.6         |
| 4    |                     | 1.0                 | 0.27                    | 0.94   | 37.76                                 | 15.8         |
| avg. |                     |                     |                         |        |                                       | 15.4         |

## VI. CONCLUSIONS

As discussed above, the  $Y_3Al_5O_{12}$  garnets coactivated with  $Tb^{3+}$  and  $Ce^{3+}$  are interesting materials in which radiative, nonradiative, and energy-transfer processes can occur simultaneously at room temperature.

A new excitation band corresponding to the  $4f-5d$  transition of  $Tb^{3+}$  occurs in the excitation spectrum of the  $Ce^{3+}$  emission. For short-wavelength uv excitation from 250 to 290 nm,  $Tb^{3+}$  ions in the YAG:Tb,Ce system are excited to the  $f^75d$  state and then decay rapidly nonradiatively to the  $^5D_3$  and  $^5D_4$  levels. Part of the excitation is then emitted as characteristic  $^5D_3, ^5D_4 \rightarrow ^7F_J$  ( $J=6, 5, \dots$ ) emissions. The excitation energy is also transferred from  $^5D_3$  and  $^5D_4$  to  $Ce^{3+}$  ions by radiative and nonradiative resonant energy transfer.

In YAG:Tb,Ce, nonradiative transfer from  $Tb^{3+}$  to  $Ce^{3+}$  depletes the populations of the excited  $^5D_3$  and  $^5D_4$

states of  $Tb^{3+}$  and decreases the emission intensity and fluorescence lifetime from those states. The mechanism governing nonradiative energy transfer from the  $^5D_3$  and  $^5D_4$  levels to the lowest  $5d$  state ( $^2D_{3/2}$ ) of  $Ce^{3+}$  is the electric dipole-dipole interaction. The dipole-quadrupole interaction is negligible at room temperature. The experimental decay curves were fitted to the Inokuti-Hirayama equation. The average critical transfer distances  $R_0$  are 15.1 Å for  $^5D_3(Tb^{3+}) \rightarrow ^2D_{3/2}(Ce^{3+})$  and 15.4 Å for  $^5D_4(Tb^{3+}) \rightarrow ^2D_{3/2}(Ce^{3+})$ , respectively.

## ACKNOWLEDGMENTS

This research was sponsored by the Chinese Academy of Sciences. The authors are indebted to Yu Baogui for help with the optical measurements and Dr. W. H. Fonger for discussions.

- <sup>1</sup>A. A. Kaminski, in *Laser Crystals—Their Physics and Properties*, translation edited by H. F. Ivey (Springer-Verlag, Berlin, 1981).
- <sup>2</sup>G. Blasse and A. Bril, *Appl. Phys. Lett.* **11**, 53 (1967).
- <sup>3</sup>K. Ohno and T. Abe, *J. Electrochem. Soc.* **133**, 638 (1986).
- <sup>4</sup>J. M. Robertson and M. W. van Tol, *Appl. Phys. Lett.* **37**, 471 (1980).
- <sup>5</sup>W. J. Miniscalco, J. M. Pellegrino, and W. M. Yen, *J. Appl. Phys.* **49**, 6109 (1978).
- <sup>6</sup>J. Mares, B. Jacquier, C. Pedrini, and G. Boulon, *Rev. Phys. Appl.* **22**, 145 (1987).
- <sup>7</sup>G. Blasse and A. Bril, *J. Lumin.* **3**, 18 (1970).
- <sup>8</sup>J. L. Sommerdijk and J. M. P. J. Verstegen, *J. Lumin.* **9**, 415 (1974).
- <sup>9</sup>C. Parent, C. Le Flem, M. Et-Tahirou, and A. Daoudi, *Solid State Commun.* **37**, 857 (1981).
- <sup>10</sup>B. Saubat *et al.*, *Mater. Res. Bull.* **16**, 193 (1981).
- <sup>11</sup>G. Balsse, *Phys. Status Solidi A* **73**, 205 (1982).
- <sup>12</sup>M. Leskelä and J. Suikkanen, *J. Less-Common Met.* **112**, 71

- (1985).
- <sup>13</sup>Xingren Liu, and Long Ma, *Lumin. Disp. Dev.* **5** (2), 93 (1984) (in Chinese).
- <sup>14</sup>Xingren Liu, Xiaojun Wang, Wufu Shun, Zhongkai Wang, and Long Ma, *J. Chin. Rare Earth Soc.* **5** (4), 15 (1987) (in Chinese).
- <sup>15</sup>Xingren Liu, Xiaojun Wang, Long Ma, Wufu Shun, and Zhongkai Wang, *J. Lumin.* **40/41**, 653 (1988).
- <sup>16</sup>J. Shmulovich, G. W. Berkstresser, and D. Brasen, *J. Chem. Phys.* **82**, 3078 (1985).
- <sup>17</sup>F. Auzel, in *Radiationless Processes*, edited by B. Di Bartolo and V. Goldberg (Plenum, New York, 1980), p. 213.
- <sup>18</sup>T. Förster, *Ann. Phys. (Leipzig)* **2**, 55 (1948).
- <sup>19</sup>D. L. Dexter, *J. Chem. Phys.* **21**, 836 (1953).
- <sup>20</sup>M. Inokuti and F. Hirayama, *J. Chem. Phys.* **43**, 1978 (1965).
- <sup>21</sup>M. Yokota and O. Tanimoto, *J. Chem. Soc. Jpn.* **22**, 779 (1967).
- <sup>22</sup>F. K. Fong and D. J. Diestler, *J. Chem. Phys.* **56**, 2875 (1972).